# Self-Assembly of an Alphavirus Core-like Particle Is Distinguished by Strong Intersubunit Association Energy and Structural Defects

**Joseph Che-Yen Wang,[†,#] Chao Chen,[†,⊥,#] Vamseedhar Rayaprolu,[‡,∥] Suchetana Mukhopadhyay,[‡] and Adam Zlotnick[*,†,‡,§]**

[†]Department of Molecular and Cellular Biochemistry, [‡]Department of Biology, [§]Department of Chemistry, Indiana University, Bloomington, Indiana 47405, United States. [#]JC-YW and CC contributed equally to this paper. [⊥]Present address: Medical University of South Carolina, Department of Radiology, 96 Jonathan Lucas Street, Charleston, South Carolina 29425, United States. [∥]Present address: Montana State University, Department of Cell Biology and Neuroscience, Bozeman, Montana 59717, United States.

**ABSTRACT** Weak association energy can lead to uniform nanostructures: defects can anneal due to subunit lability. What happens when strong association energy leads to particles where defects are trapped? Alphaviruses are enveloped viruses whose icosahedral nucleocapsid core can assemble independently. We used a simplest case system to study Ross River virus (RRV) core-like particle (CLP) self-assembly using purified capsid protein and a short DNA oligomer. We find that capsid protein binds the oligomer with high affinity to form an assembly competent unit (U). Subsequently, U assembles with concentration dependence into CLPs. We determined that U—U pairwise interactions are very strong (*ca.* −6 kcal/mol) compared to other virus assembly systems. Assembled RRV CLPs appeared morphologically uniform and cryo-EM image reconstruction with imposed icosahedral symmetry yielded a $T = 4$ structure. However, 2D class averages of the CLPs show that virtually every class had disordered regions. These results suggested that irregular cores may be present in RRV virions. To test this hypothesis, we determined 2D class averages of RRV virions using authentic virions or only the core from intact virions isolated by computational masking. Virion-based class averages were symmetrical, geometric, and corresponded well to projections of image reconstructions. In core-based class averages, cores and envelope proteins in many classes were disordered. These results suggest that partly disordered components are common even in ostensibly well-ordered viruses, a biological realization of a patchy particle. Biological advantages of partly disordered complexes may arise from their ease of dissociation and asymmetry.

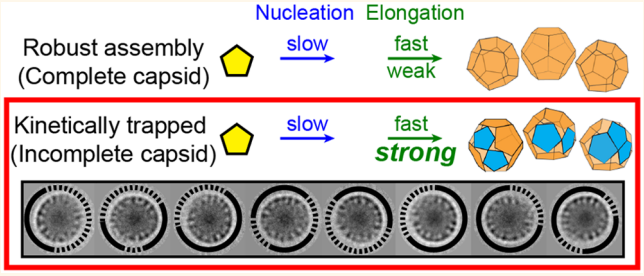


**KEYWORDS:** Ross River virus · capsid · self-assembly · enveloped viruses

About half of known virus families have a spherical (icosahedral) capsid that is composed of tens to thousands of identical subunits. In most of these viruses, subunits are arranged with a quasi-equivalence to make a characteristic pattern of pentamers and hexamers.[1]

Viruses are an example of an evolved, optimized self-assembling nanoparticle. However, generalizations for nanoparticle assembly should apply equally to viruses, other biological complexes, and abiological nanoparticles. Numerous studies suggest that assembly is based on weak subunit−subunit association energy (Figure 1A).[2−4] Weak intersubunit contacts provide the opportunity to thermodynamically correct mistakes to yield a well-ordered product. The resulting complexes, where every multivalent subunit is maximally ligated, have a high barrier to dissociation allowing them to persist even at low concentration. This behavior is ideal for viruses where capsid integrity is critical for infection (*e.g.*, extracellular picornaviruses or intracellular transport of hepadnavirus cores to the nucleus).[5] Defects creep into assembly simulations when nucleation is fast compared to elongation or when intersubunit interactions are strong, resulting in trapped intermediates (Figure 1B).[4,6] Formation of trapped incomplete particles can be engineered into particle assembly.[7] A third

* Address correspondence to azlotnic@indiana.edu.

Received for review May 1, 2015 and accepted August 14, 2015.

**Published online August 14, 2015**
**10.1021/acsnano.5b02632**

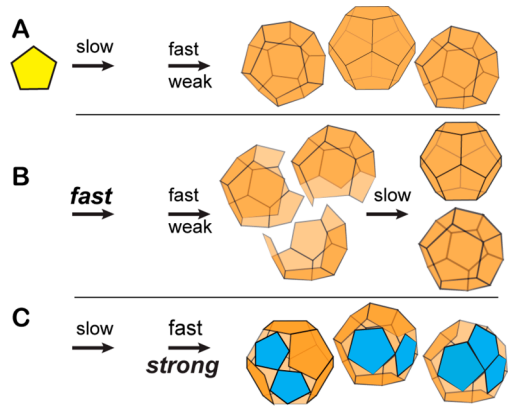


**Figure 1. Models of capsid assembly and trapped assembly. For simplicity, we consider assembly of a dodecahedron; the first arrow indicates the rate of nucleation, the second indicates the rate of elongation (above the arrow) and average association energy (below the arrow).[5,43] Changes in assembly kinetics or thermodynamics are bolded. (A) Assembly is robust when nucleation is relatively slow, elongation fast, and association weak. In this regimen, subunits that add with incorrect geometry readily dissociate to eliminate defects. (B) Incomplete capsids can be trapped when nucleation is relatively fast resulting in so many nuclei that there is insufficient free subunit to complete the nascent capsids. Incomplete capsids can also be trapped with high association energy or high protein concentration. Incomplete capsids can slowly cure by exchange of subunits.[6,7] (C) Capsids can become mosaic when association is fast enough or strong enough to prevent dissociation of subunits with incorrect geometry (blue subunits). Defects will be common when there is a deep local energy minimum for an alternative geometry for subunit−subunit interaction.**

assembly model adds low energy alternative geometries for intersubunit interaction to yield mosaic lattices that do not have quasi-equivalence (Figure 1C).[8,9] Examples of viruses with alternative subunit−subunit interactions include pseudo-$T = 2$ bromoviruses under aggressive assembly conditions.[10,11] Immature human immunodeficiency virus (HIV) provides an example of assembly with numerous trapped defects.[12,13]

We chose to evaluate assembly of alphavirus capsid protein (CP) because of the ease of controlling assembly, the apparent lability of particles, and the ease of correlating biophysical and biological observations with this system.[14−16] Alphaviruses are enveloped, positive strand RNA viruses that are cyclically transmitted between arthropod vectors and a wide range of vertebrate hosts including humans.[17,18] In both hosts, alphavirus replication and assembly occur in the cytoplasm. Prototype alphaviruses include Sindbis and Ross River virus (RRV). The virion is a ~ 70 nm diameter particle comprised of a ~ 40 nm nucleocapsid core, a lipid bilayer, and glycoprotein spikes. The core and glycoprotein layers share $T = 4$ icosahedral symmetry.[19−23] The nucleocapsid core consists of 240 copies of capsid protein (CP) and the viral genome. *In vivo*, one mechanism of alphavirus assembly has independent pathways for core assembly and formation of envelope protein complexes, which merge during budding from the plasma membrane to form mature virion particles.[24−26]

Alphavirus CPs are highly conserved[27] and can be divided into the N- and C-terminal domains. The N-terminus includes ~30 basic residues (27 in RRV)[28−30] and an 18-amino-acid region predicted to form a coiled-coil motif.[15] The C-terminal domain has a chymotrypsin-like domain and a hydrophobic pocket that interacts with the cytoplasmic domain of the E2 glycoprotein.[26,31−33] In cryo-EM structures of virions, the CP N-terminal residues are disordered while the C-terminal domain can be modeled into density.[19−21,23,34] *In vitro*, alphavirus CP requires polyanionic cargo to form core-like particles (CLPs); the protein alone will not self-assemble in response to ionic strength or pH at any concentration yet tested.[16,35−39] *In vitro*-assembled CLPs are structurally and functionally similar to cores of mature virions[14,16] as they appear to have $T = 4$ symmetry and are able to interact with viral glycoproteins[26,40−42] to form functional virus-like particles.[41,42]

Assembly of closed spherical capsids has been characterized by weak subunit−subunit interactions and disassembly under stringent conditions.[3,6,43] Examples include hepatitis B virus (HBV) and cowpea chlorotic mottle virus. However, in the present study, we found that *in vitro* alphavirus core assembly follows a different paradigm. We observed strong subunit−subunit interactions but the resulting CLPs readily disassembled. Consistent with these observations, we found that most CLPs had geometric defects. We also found evidence for "imperfect" cores in mature virions. We propose that irregular cores may be common in enveloped viruses where capsid structural integrity is not critical for (and may be detrimental to) the virus lifecycle.

## RESULTS AND DISCUSSION

**CP and DNA Form a Complex That Assembles into Capsids.** The goal of the initial studies was to measure CP-CP interaction. We drove assembly with a single-stranded 27mer DNA oligonucleotide. The charge on this short oligo is sufficient to neutralize the N-terminal basic residues of RRV CP, but yet not long enough to cross-link CP subunits or act as a scaffold for binding multiple CP monomers. This system was used to allow assembly to proceed *via* freely diffusing monomers. Previous studies showed that short oligos supported assembly though not as well as oligonucleotides that could bind several subunits.[16]

Assembly was measured by static and dynamic light scattering. The intensity of the light scattered by a solute (static light scattering) is proportional to the average molecular weight of the sample. Fluctuations of the light scattering signal (dynamic light scattering or DLS) are proportional to the diffusion coefficient of the solute and thus its hydrodynamic diameter. Solutions of 1.5 $\mu$M RRV CP were titrated with the DNA 27mer and monitored by static light scattering and DLS (Figure 2A). Unassembled, monomeric RRV CP

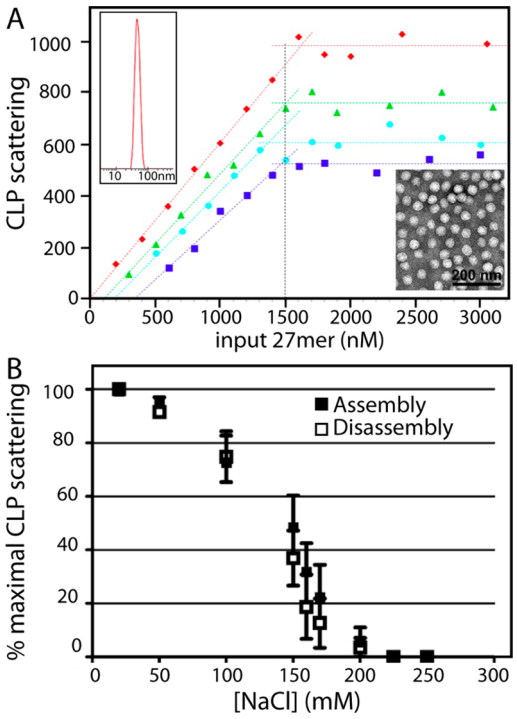


**Figure 2.** *In vitro* **assembly of RRV CLPs is sensitive to ionic strength. (A) Static light scattering measurement of titrations of 1.5 $\mu$M RRV CP by a 27mer DNA oligo (DLS and TEM in Figures S1−S5). Samples were at 22 °C at various ionic strengths (red = 50 mM NaCl, green = 110 mM NaCl, cyan = 150 mM NaCl, and blue = 170 mM NaCl). Data were fit to two straight lines. The pseudocritical concentration (X-intercept) was determined from this linear fit. In each data set, the RRV CP saturated at about one 27mer DNA oligo per protein. The dotted black vertical line marks where when equimolar amounts of RRV CP and 27mer DNA oligo are mixed. (B) CLPs show no hysteresis. Either CLPs were assembled in increasing concentrations of NaCl (closed squares) or preassembled CLPs were disassembled by diluting to lower concentrations of NaCl (open squares). The amount CLP present, measured by light scattering as ionic strength changes, is almost identical for assembly and disassembly.**

molecules had weak static light scattering and a DLS-estimated diameter of ~9 nm (Figure S1). The 27mer DNA, at the concentrations used in this work, did not detectably increase the amount of scattered light above background. In titrations of RRV CP by 27mer, light scattering intensity increased and DLS analysis indicated a diameter of 40−50 nm (Figures S2−S5) corresponding to RRV CLPs. In some DLS analyses, large diameter peaks beyond the capsid peak were noted, but these aggregates represented a small amount of the total mass, were irregular in size, were not reproducible, and made little contribution to light scattering intensity. We confirmed the presence of CLPs by TEM (Figure S1). The diameter of RRV CLPs, from negative stain TEM, agrees well with RRV CLPs measured by DLS and nucleocapsid cores from intact virus particles.[14,16,19,22,44]

The dependence of CLP assembly on the concentration of 27mer DNA was determined by static light scattering (Figure S2−S5) at different NaCl concentrations

**TABLE 1. Association of U to Form CLP**

| [NaCl] (mM) | $K_D$apparent (nM) | $\Delta G_{contact\ \ intersubunit}$ (kcal/mol)[a] |
|---|---|---|
| 50 | 0 | tight binding |
| 110 | 108 | −6.25 |
| 150 | 186 | −6.13 |
| 170 | 345 | −5.80 |

[a] Values are from Figure 2A. For this calculation, we assume U is an asymmetric monomer, making 3 contacts ($c = 3$, $J = 1$) and forms a $T = 4$ capsid ($N = 240$) (see eq 14.9 in ref 43).

(Figure 2A). We observed that a minimum concentration of DNA was needed to initiate CLP assembly (the X-intercept in Figure 2A, Table 1). Below this pseudocritical concentration there was no measurable CLP (scattering intensities were at noise level and no stable or reproducible DLS peaks were observed), and above it CLP concentration increases linearly with input DNA until it saturates RRV CP at equimolar. With the rising ionic strength, the pseudocritical concentration increases while the maximum CLP assembly decreases, suggesting that it is consistent with the requirement of anionic cargo for the formation of CLPs because the interactions between CP-DNA complexes have electrostatic contributions.

From these data, we propose a minimal assembly model where one RRV CP molecule binds to one 27mer oligo to yield an assembly subunit (U), 240 of which can go on to form a CLP. Based on the assembly maximum at an RRV CP:DNA oligo ratio of 1:1 it appears that oligo-binding is essentially quantitative in this concentration range (Figure 2A).

$$240(\mathrm{CP} + \mathrm{oligo}) \leftrightarrow 240\mathrm{U} \leftrightarrow \mathrm{CLP} \qquad (1)$$

This model (eq 1) is readily analyzed when 27mer binding is quantitative and the concentration of CLP varies as a function of the U−U association energy as described by the mass action law for $K_{capsid}$ (eq 2).[6,43] $K_{capsid}$ is related to the observed pseudocritical concentration of assembly, $K_D$apparent. Physically, $K_D$ apparent is the equilibrium concentration where the concentrations of free U and U in CLP are equal ($K_D$ apparent = [U] = 240[CLP]). Thus, at concentrations above $K_D$apparent, addition of oligo results in CLP formation until the protein concentration is saturated.

$$K_{capsid} = \frac{[\mathrm{CLP}]}{[\mathrm{U}]^{240}} = \frac{1}{240K_D\mathrm{apparent}^{239}} \qquad (2)$$

$K_{capsid}$ can be deconstructed to the pairwise association constants between individual subunits (Table 1),[6,43] taking into account that there are 240 subunits in a $T = 4$ capsid each making three intersubunit contacts. A minimum of three contacts is required for forming a 2D lattice and is consistent with the structure of the CLP.[14] The resulting association energies between U subunits include contributions from protein−protein and protein-nucleic acid interactions. The nucleic acid may

specifically neutralize charge of one CP or may make other contributions to CLP formation.

**CLP Formation Shows No Detectable Hysteresis to Disassembly.** Virus capsids are closed polymers, once complete there is no "edge" to facilitate equilibration between free and bound subunits, which creates an inherent hysteresis to dissociation.[45−47] Thus, a simple test for the completeness of a capsid is to compare the ionic strength dependence of assembly and disassembly. If the curves do not overlap it is indicative of hysteresis.

We observed that increasing ionic strength affected CLP stability (Table 1, Figure 2B). To test for hysteresis in RRV CLPs we examined how ionic strength affected stability of preassembled particles compared to spontaneous assembly at the same ionic strength (Figure 2B). RRV CP and oligo were assembled in buffers of varying NaCl concentrations and compared to disassembly of preformed 1:1 RRV CP:oligo CLPs. Within error, assembly and disassembly showed the same sensitivity to ionic strength for samples measured with 1 h of mixing. Between 50 and 200 mM NaCl, CLP stability decreased monotonically. The similarity in ionic strength dependence for both assembly and disassembly was observed regardless of initial RRV CP starting concentration. By comparison, samples of hepatitis B virus capsid protein can persist in the capsid form for months under conditions where they could not assemble.[45,48]

***In Vitro* Assembled CLPs Are Heterogeneous.** The lack of hysteresis for disassembly suggested that our CLPs had defects.[6,45,46] A 3D image reconstruction of CLPs had previously been published[14] and its low resolution suggested inherent heterogeneity between the particles. Our CLPs in cryo micrographs had spherical morphology with a small number of distorted or smaller particles (Figure 3A). Translationally aligned averaged cryo images show the capsid has an outer diameter of about 38 nm surrounding a weaker internal density layer (Figure 3A, inset), similar to the nucleocapsid in intact Sindbis virus.[20,49] We determined a 3D image reconstruction of our CLPs to 17.9 Å resolution, using the nucleocapsid core from an RRV reconstruction (Figure S6) low-pass filtered to 40 Å to bootstrap particle orientation (Figures 3B, C). This structure shows the well-organized hexamers and pentamers connected to one-another by weaker density as seen in other alphavirus and alphavirus CLP structures.[14,19−23,44] However, 3D reconstruction imposes symmetry during the alignment process; it shows the presence of a common structural lattice but necessarily obscures irregularities by icosahedral averaging.

To test for particle fidelity and uniformity, we examined the CLP images using unbiased 2D classification. Previously, we used 2D classification to identify incomplete kinetically trapped hepatitis B virus capsids, where we found that incomplete particles favored a limited number of discrete sizes.[7] We reasoned that

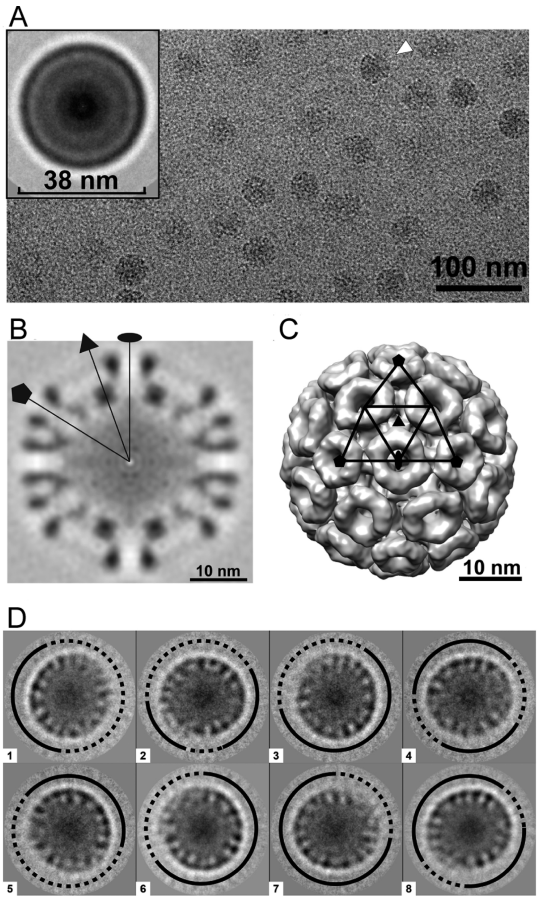


**Figure 3. The structure of Ross River virus CLPs shows a mixture of complete and partially complete spherical particles. (A) A cryo-micrograph of RRV CLPs shows many spherical and some distorted particles (white arrow). A translationally aligned averaged image (inset) shows that the RRV CLPs have an average diameter of ~38 nm. (B) The central section of an 17.9 Å resolution 3D reconstruction of an RRV CLP. The oval, triangle, and pentagon indicate locations of 2-fold, 3-fold and 5-fold axes, respectively. (C) A surface-shaded representation of the RRV CLP rendered at 1$\sigma$ above the average density, viewed along the icosahedral 2-fold axis. The CLP shows a $T = 4$ organization. For this reconstruction, icosahedral symmetry was imposed. (D) Reference-free class averages of RRV CLPs. Classes show irregularities (compare solid and dashed lines) on the CLP surface.**

reference-free 2D classification would allow CLP defects, not necessarily visible in the raw data, to align.[7] Class averaging also allows us to overcome some of the noise inherent in cryo-microscopy at the expense of averaging away some dissimilarities within a class, understating the actual differences. Nonetheless, we observed that a large fraction of particles had partially disordered regions evident in class averages by diffuse density at the capsid surface while the other regions were well demarcated indicating structural order (Figure 3D). This indicates a heterogeneous population of CLPs containing partially organized RRV CP subunits, providing a basis for the lack of hysteresis and fragility observed here and previously.[14]

**Nucleocapsid Cores in Virions Share Properties with *in Vitro* Assembled CLPs.** We hypothesized that high association

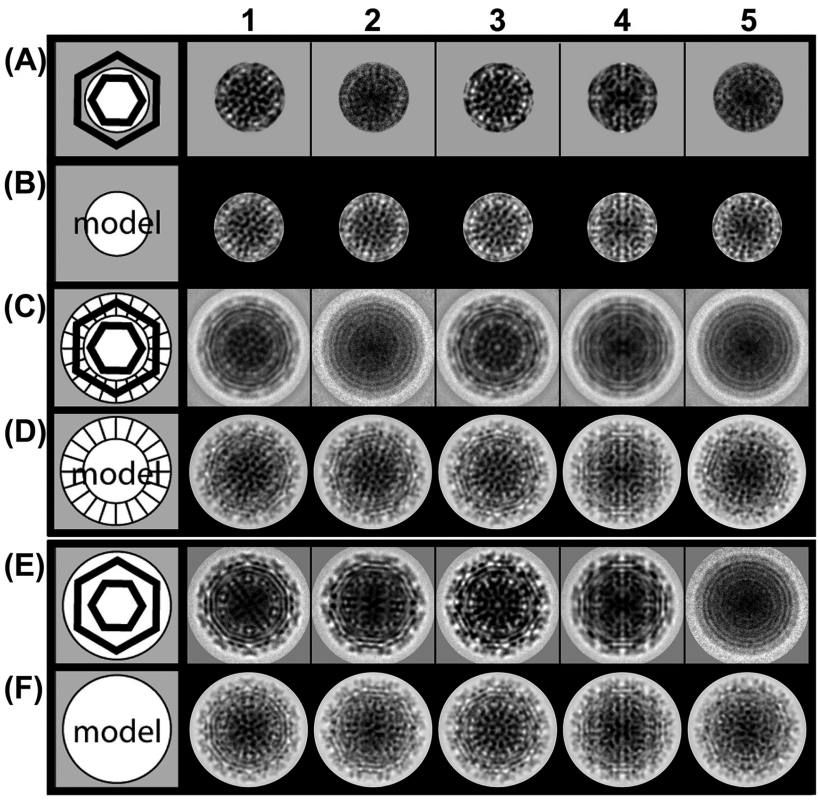


**Figure 4. Selected virion class averages show evidence of core disorder. A group of 6560 images of freshly prepared RRV virions were grouped into 12 classes (see Figure S7 for the complete set) and compared with a 3D model. (A) Experimental core-based class averages used only the core for the class averaging. The schematic of a virion (left most column) shows the glycoprotein masked out (gray area). (B) The nucleocapsid density from a 3D reconstruction of RRV was isolated computationally (white area of cartoon) and projections were calculated to best match the class averages in row A. (C) Experimental class averages of RRV virions, classified and aligned based on their cores from row A, but including the glycoprotein layer. The hashed outer ring in the cartoon indicates that the glycoprotein layer is shown in the images to the right but not used for classification. In several classes the envelope is regular and geometric (*e.g.*, column 1). In others, it is misaligned resulting in concentric circles (*e.g.*, column 2). (D) To mimic the images in row C, projections were calculated using the entire RRV image reconstruction and the orientations from row B. In these projections, the glycoprotein envelopes are distinctly geometric, even in cases where row C showed an irregular core. (E and F) In control experiments, classification of RRV based on the entire virion (E) generally shows a well-organized periphery (*i.e.*, the glycoprotein layer) and matches well with corresponding projections of the RRV image reconstruction (F). The core region of E generally appears to be well-organized. However, here are some classes that appear poorly organized (*e.g.*, column 5).**

energy between subunits would lead to a propensity for CLP defects and this was experimentally supported by observations (Figure 2B, 3). Previous work has demonstrated that CLPs interact with glycoproteins and these particles function like mature virions.[26,41,42] If cores with defects are the standard, then similar defects seen in CLP particles should be observed in virions. Indeed, while the envelope proteins may cause some rearrangement of the CP during budding,[26,50] if the defects seen in the CLPs are observed in virions, then envelope proteins do not completely reorganize the core particle. Because the inner core and outer glycoprotein layers of alphaviruses are aligned,[19−21,23,34] we reasoned that class averages based on virion cores should yield the same results as class averages based on the whole virus if, and only if, the cores provided sufficient signal and were organized. If the class averages were different between the cores and the entire particle, then the cores are either not intact or have a different organization compared to the glycoprotein spikes. Because of the lack of regularity of anticipated defects, this test will undercount partially disorganized cores.

To focus on the core and minimize contribution of the glycoprotein envelope, reference free class averages were determined by limiting the data used in classification to a radius of $\leq$22 nm (Figure 4A). 6560 cryo-EM images of virions were separated into 12 classes. Class averages of the core region compared to varying degrees with projections of core density (from a 15 Å resolution RRV image reconstruction (Figure S6B)) were aligned to achieve the best match (Figures 4B and S7). Most of the class averages (Figure 4A) and projections (Figure 4B) showed matching geometrical features but a substantial fraction did not.

To examine how well the glycoprotein envelopes were aligned with cores, images in the core-based class averages (Figure 4A) and model projections (Figure 4B) were expanded to include the glycoprotein layers (Figure 4C, D). In the projections, the highly geometric

features of the glycoprotein layer were unambiguous (Figure 4D). The similarities and differences between the class averages and the projections were striking (Compare Figure 4C and 4D). For example, in the class shown in column 1, the correspondence between the project and class average were good for both the core (rows A and B) and the whole virus (rows C and D). On the other hand, column 2 tells a different story: the class average and the core projection appear consistent (compare rows A and B), but the glycoprotein layer, averaged over the class, is so misaligned that it is reduced to featureless concentric circles. We see evidence of this disconnect in 40% of the particles, based on class averages (classes 2, 4, 5, 8, 11, and 12 in Figure S7). To examine the organization of the whole virion for comparison to the core-based averages, the same images were sorted into classes using a cutoff radius of 37 nm to include the envelope with minimal background (Figure 4E). Most, but not all, of these averages (accounting for 88% of the images) show detailed geometrical features at high radius consistent with a well-ordered glycoprotein layer. The geometrical averages correspond extremely well with projections (Figure 4F).

Strikingly, in some cases, the core in the core-based class average (column 4, rows A−D) matches very well with the core in the glycoprotein-based class (column 4, rows E−F). However, the glycoprotein layer for the core-based averages is poorly ordered (row C).

Taken together, it appears that virion-based class averages, dominated by the glycoprotein layer, generally yield ordered results. A small fraction of viruses (12%) were in virion-based class averages that had featureless glycoprotein layers, suggestive of irregular particles. A larger fraction of core-based class averages showed weak alignment of the glycoprotein layers. To the best of our knowledge, this is the first example where masked 2D class averages have been used to look for defective virus components. This result suggests that cores in particular, as well as some viruses, have a heterogeneity of organization inconsistent with icosahedral symmetry. It is not clear how symmetry correlates with infectivity. For RRV from BHK cells, the ratio of particles to plaque forming units is anywhere from 100 to 500. We cannot distinguish whether infectivity is attributable to a particular subset of asymmetric particles, the rare symmetrical particles, or particles that have some specific feature not readily obvious from this analysis.[51]

**Context for a High-Error Assembly Model.** In summary, we quantitatively described alphavirus CLP assembly and disassembly with a minimal system composed of RRV CP and a short DNA oligomer, where the DNA had sufficient charge to neutralize the RRV CP RNA-binding domain;[52−54] in addition to nucleotide binding, RRV CLP assembly appears to include attractive electrostatic interactions (Table 1). We determined that RRV CP-DNA subunits had a pairwise association energy of approximately −6 kcal/mol per pairwise contact (Table 1), much stronger than the typical value of −3 to −4 kcal/mol observed for other viruses.[5,6,46] We observed no evidence of hysteresis between assembly and disassembly (Figure 2B). While assembled CLPs had $T = 4$ organization (Figure 3), we discovered many had defects or disordered regions. We found evidence that a fraction of RRV virions also have irregular cores, correlating our biophysical study with biology (Figure 4).

All of our results are consistent with a CLP that has flaws in its geometry. We suggest that these arise from subunits assembling incorrectly due to strong association energy between subunits. In simulations, when individual interactions between capsid subunits are weak, "incorrect" subunits can dissociate and reassociate correctly (thermodynamic editing); conversely, when association energy is strong, defects in the packing of subunits are anticipated because subunits become trapped and the growing complex cannot self-repair (Figure 1C).[6,46,55] Conceptually, this can create a mosaic capsid, a capsid with defects, regions of order and disorder, and even alternative lattices. We observe evidence that many RRV CLPs and cores do not form an ideal shell (Figures 3D, 4A, and C). The icosahedral averaging used to determine structures can disguise these geometric flaws, giving an impression of perfect symmetry.

An intact core is not actually necessary for the construction of an alphavirus-like particle. This was demonstrated with a Semliki Forest virus mutant that carried a capsid protein with defects in protein−protein interaction.[56] The mutant virus formed an enveloped nucleoprotein complex in which the glycoprotein envelope was nearly identical to that of wild type virion and the core was largely disordered although the virus-like particles had the correct stoichiometry of components. Similar organized glycoprotein layers and disorganized cores are seen in flaviviruses (*e.g.*, West Nile and Dengue).[57,58] High-resolution icosahedrally averaged structures are available for two alphaviruses, Chikungunya virus[23] and Venezuelan Equine Encephalitis virus.[19] As with lower resolution virion structures, intracapsomer contacts (5-fold and quasi-6-fold complexes) were more apparent than intercapsomer contacts. Well-defined interactions were also found between the core and the cytoplasmic domain of glycoprotein E2, suggesting an ordering influence.[26,32,33,40] In the Chikungunya virus structure the core density is weaker than that of the glycoprotein and the first ~115 residues are disordered. Indeed, they have been suggested to form a nonicosahedral internal scaffold.[23]

Closed, spherical capsids may be advantageous when the capsid is exposed to destabilizing

environments, *e.g.*, during transmission (Figure 1A). We suggest that capsid integrity correlates with particle persistence. For viruses that rely on their envelope for stability and envelope proteins for the transmission, a different assembly mechanism (Figure 1C) may be advantageous. We speculate that there is a biological advantage to RRV capsids with structural defects. In the virion, the nucleocapsid core appears to be a well-ordered, closed shell. Indeed, interaction with well-ordered glycoprotein may correct the misassembled capsids.[56] However, once the nucleocapsid core is released into the cytoplasm a flawed capsid can readily disassemble. A virus would not survive if being "sloppy" did not provide an evolutionary advantage.

Assembly of virus capsids is not restricted to weak interactions. However, when viruses use strong interactions we find the irregularity predicted from models.[3−6,8,46,47,59,60] Irregularity is not necessarily a bad thing. Models based on cones, irregular structures, and spheres show that novel interactions will be accommodated.[8,9,59] Biology clearly accommodates defects.[10−13] Advantages of a mosaic particle include responsiveness to a destabilizing environment and also provide a basis for asymmetry from a symmetric lattice.

## METHODS

**Expression and Purification of Ross River Capsid Protein (RRV CP).** Ross River virus capsid protein (RRV CP) was cloned into a pET29b, expressed in Rosetta 2 cells (Novagen, EMD Chemical Inc. Gobbstown, NJ) and purified as described previously (Figure S8).[35,42] For the protein samples used in the dissociation experiments, the lysis, loading, and elution buffer at pH 6.8 rather than pH 7.5 were subsequently concentrated and exchanged into 20 mM HEPES, pH = 7.4, 150 mM NaCl, and 0.1 mM EDTA using Vivaspin 2 filters with a 10 kDa cut of filter (Vivaproducts, Inc., Littleton, MA). The protein concentration was determined by absorbance using an extinction coefficient of 39 670 $M^{-1}$ $cm^{-1}$ at 280 nm. Concentrated protein was aliquoted and stored at 4 °C or −20 °C; frozen aliquots were not thawed more than twice.

**Core-like Particle (CLP) Formation.** For assembly titrations, CP at a final concentration of 1.5 $\mu$M was mixed with 27mer single-stranded DNA oligo (5′-TAC CCA CGC TCT CGC AGT CAT AAT TCG). For these reactions, the NaCl concentration was varied as described in text. For comparisons of assembly and disassembly, CLPs were assembled by adding 1−3 $\mu$M of RRV CP to DNA oligo in the appropriate ionic strength. In disassembly reactions, CLPs were assembled at 0 mM NaCl and aliquots diluted into buffer containing NaCl. The extent of assembly was determined by static light scattering, dynamic light scattering, and transmission electron microscopy.

**Light Scattering and Dynamic Light Scattering (DLS).** Light scattering and DLS experiments were performed with Malvern Zetasizer Nano ZS ZEN3600 at 22 °C using the manufacturer's quartz cuvette, ZEN2112. Light scattering is reported as "raw" counts from this instrument. Particle size information was determined using the manufacturer's software. Each measurement consisted of at least 10 measurements and triplicate samples. Each experiment was reproduced using at least two different protein preparations.

**Virus Purification.** RRV was generated by electroporating BHK cells with T48 strain of Ross River virus as described previously.[61] 24 hours post electroporation the media was collected and cell debris was removed by centrifugation. The media was spun at 5000*g* overnight at 4 °C. The media was removed and the pellet was resuspended in 20 mM HEPES, pH 7.4, 150 mM NaCl, and 0.1 mM EDTA. When necessary, virions were concentrated using Vivaspin 6 100 kDa filters at 5000*g* at 4 °C.

**Transmission Electron Microscopy (TEM).** For negative stained EM, sample was applied to a hydrophilic glow-discharged carbon-coated 300-mesh copper grid and stained with 2% uranyl acetate. Images were acquired on an 80 kV JEOL-1010 transmission electron microscopy equipped with a Gatan 4 k × 4 k CCD camera.

For cryo-EM, sample was applied to glow-discharged 300-mesh copper grids and plunge-frozen using an FEI Vitrobot. Cryo-images were collected using a 300 kV JEOL-3200FS electron microscope with an in-column energy filter at a nominal magnification of 60 000× (equal to 1.84 Å per pixel at the specimen space). Exposure was less than 25 $e^{-}/Å^2$ to avoid beam-induced damage. Images with minimal specimen drift and astigmatism were selected for further analysis. Reconstructions were calculated using EMAN2 and AUTO3DEM software as previously described.[62−64] For RRV virion, 6829 particles were initially selected and the initial model was built de novo. The final 3D reconstruction, computed from 6146 particles, was estimated to 15 Å in resolution using a Fourier Shell Correlation (FSC) of 0.5. For the RRV CLP (Figure 3B, C), the initial model was based on the nucleocapsid layer (radii of 12−22 nm) of the cryo-EM density map of the RRV virus low pass filtered to 40 Å. In total, 4124 particles were selected and 3713 particles were used in the final 3D reconstruction. The resolution was estimated to be 17.9 Å based on a FSC of 0.5. The 3D reconstructions were rendered and visualized using RobEM[65] and UCSF Chimera.[66] The 2D reference-free classification was computed using XMIPP.[67] The glycoprotein layer of the 3D model of RRV virus was masked by using PCUT program to remove the density beyond radius of 22 nm. To mask the glycoprotein layer of the 2D images of RRV virus, the particle images were first centered using Cenalignint[68] and then masked by xmipp_transform_mask to remove the density beyond 22 nm in radius. The correlation coefficient between model projections and class averages were calculated using Parallel Polar Fourier Transform (PPFT) program, part of the AUTO3DEM software.

The masked particles allowed us to make predictions for different scenarios. If the particles were well-ordered, we would see well-defined arrangement of density. If the particles had defects with a specific geometric relationship to the underlying icosahedral symmetry, we would expect to see partially organized and partially smeared density. If the particles had random defects we would expect classification to fail completely resulting in a smeared ring. We have used this method to identify incomplete particles in kinetically trapped HBV capsid assembly reactions. For ordered virions consistent with symmetrized reconstructions, we expected both glycan and core layers to show order in common orientations. Whereas cores with defects would have a tendency to allow alternative orientations for the glycan layer, resulting in disordered core or glycan layers.

The cryo-EM density maps reported in this paper have been deposited in the EMDataBank database. The accession number for RRV CLP is EMD-2964 and for RRV virion is EMD-2965.

*Conflict of Interest:* The authors declare the following competing financial interest(s): AZ is associated with a biotech startup company.

*Acknowledgment.* This research was supported by the NSF through Award MCB 1157716 to SM and the NIH through R56-AI077688 to AZ. We thank the Electron Microscopy Center at Indiana University. We also recognize the Indiana University cyberinfrastructure, which was supported in part by Lilly Endowment, Inc., through its support for the Indiana University Pervasive Technology Institute, and in part by the Indiana METACyt Initiative. The Indiana METACyt Initiative at IU is also supported in part by Lilly Endowment, Inc.

*Supporting Information Available:* The Supporting Information is available free of charge on the ACS Publications website at DOI: 10.1021/acsnano.5b02632.

DLS and EM data for a typical sample of CLPs (S1). DLS size data for titrations at various NaCl concentrations (S2−S5). A reconstruction of RRV showing a surface shaded view, a central section, and resolution data (S6). A full set of class averages (some of which are displayed in Figure 4) for CLPs and virions (S7). (PDF)

## REFERENCES AND NOTES


1. Caspar, D. L.; Klug, A. Physical Principles in the Construction of Regular Viruses. *Cold Spring Harbor Symp. Quant. Biol.* **1962**, *27*, 1–24.
2. Katen, S. P.; Chirapu, S. R.; Finn, M. G.; Zlotnick, A. Trapping of Hepatitis B Virus Capsid Assembly Intermediates by Phenylpropenamide Assembly Accelerators. *ACS Chem. Biol.* **2010**, *5*, 1125–1136.
3. Perlmutter, J. D.; Hagan, M. F. Mechanisms of Virus Assembly. *arXiv* **2014**, 1407preprint arXiv:1407.3856.
4. Whitesides, G. M.; Boncheva, M. Beyond Molecules: Self-Assembly of Mesoscopic and Macroscopic Components. *Proc. Natl. Acad. Sci. U. S. A.* **2002**, *99*, 4769–4774.
5. Zlotnick, A.; Mukhopadhyay, S. Virus Assembly, Allostery and Antivirals. *Trends Microbiol.* **2011**, *19*, 14–23.
6. Zlotnick, A. Are Weak Protein-Protein Interactions the General Rule in Capsid Assembly? *Virology* **2003**, *315*, 269–274.
7. Pierson, E. E.; Keifer, D. Z.; Selzer, L.; Lee, L. S.; Contino, N. C.; Wang, J. C.; Zlotnick, A.; Jarrold, M. F. Detection of Late Intermediates in Virus Capsid Assembly by Charge Detection Mass Spectrometry. *J. Am. Chem. Soc.* **2014**, *136*, 3536–3541.
8. Zandi, R.; Reguera, D.; Bruinsma, R. F.; Gelbart, W. M.; Rudnick, J. Origin of Icosahedral Symmetry in Viruses. *Proc. Natl. Acad. Sci. U. S. A.* **2004**, *101*, 15556–15560.
9. Chen, T.; Zhang, Z.; Glotzer, S. C. A Precise Packing Sequence for Self-Assembled Convex Structures. *Proc. Natl. Acad. Sci. U. S. A.* **2007**, *104*, 717–722.
10. Krol, M. A.; Olson, N. H.; Tate, J.; Johnson, J. E.; Baker, T. S.; Ahlquist, P. Rna-Controlled Polymorphism in the in Vivo Assembly of 180-Subunit and 120-Subunit Virions from a Single Capsid Protein. *Proc. Natl. Acad. Sci. U. S. A.* **1999**, *96*, 13650–13655.
11. Johnson, J. M.; Tang, J.; Nyame, Y.; Willits, D.; Young, M. J.; Zlotnick, A. Regulating Self-Assembly of Spherical Oligomers. *Nano Lett.* **2005**, *5*, 765–770.
12. Briggs, J. A.; Riches, J. D.; Glass, B.; Bartonova, V.; Zanetti, G.; Krausslich, H. G. Structure and Assembly of Immature Hiv. *Proc. Natl. Acad. Sci. U. S. A.* **2009**, *106*, 11090–11095.
13. Yu, Z.; Dobro, M. J.; Woodward, C. L.; Levandovsky, A.; Danielson, C. M.; Sandrin, V.; Shi, J.; Aiken, C.; Zandi, R.; Hope, T. J.; *et al.* Unclosed Hiv-1 Capsids Suggest a Curled Sheet Model of Assembly. *J. Mol. Biol.* **2013**, *425*, 112–123.
14. Mukhopadhyay, S.; Chipman, P. R.; Hong, E. M.; Kuhn, R. J.; Rossmann, M. G. In Vitro-Assembled Alphavirus Core-Like Particles Maintain a Structure Similar to That of Nucleocapsid Cores in Mature Virus. *J. Virol.* **2002**, *76*, 11128–11132.
15. Perera, R.; Owen, K. E.; Tellinghuisen, T. L.; Gorbalenya, A. E.; Kuhn, R. J. Alphavirus Nucleocapsid Protein Contains a Putative Coiled Coil Alpha-Helix Important for Core Assembly. *J. Virol.* **2001**, *75*, 1–10.
16. Tellinghuisen, T. L.; Hamburger, A. E.; Fisher, B. R.; Ostendorp, R.; Kuhn, R. J. In Vitro Assembly of Alphavirus Cores by Using Nucleocapsid Protein Expressed in Escherichia Coli. *J. Virol.* **1999**, *73*, 5309–5319.
17. Strauss, J. H.; Strauss, E. G. The Alphaviruses: Gene Expression, Replication, and Evolution. *Microbiol. Rev.* **1994**, *58*, 491–562.
18. Kuhn, R. J., Togaviradae: The Viruses and Their Replication. In *Fields' Virology*; Knipe, D. M., Howley, P. M., Eds.; Lippincott Williams: Philadelphia, PA, 2007; pp 1001−1022.
19. Zhang, R.; Hryc, C. F.; Cong, Y.; Liu, X.; Jakana, J.; Gorchakov, R.; Baker, M. L.; Weaver, S. C.; Chiu, W. 4.4 a Cryo-Em Structure of an Enveloped Alphavirus Venezuelan Equine Encephalitis Virus. *EMBO J.* **2011**, *30*, 3854.
20. Tang, J.; Jose, J.; Chipman, P.; Zhang, W.; Kuhn, R. J.; Baker, T. S. Molecular Links between the E2 Envelope Glycoprotein and Nucleocapsid Core in Sindbis Virus. *J. Mol. Biol.* **2011**, *414*, 442–459.
21. Kostyuchenko, V. A.; Jakana, J.; Liu, X.; Haddow, A. D.; Aung, M.; Weaver, S. C.; Chiu, W.; Lok, S. M. The Structure of Barmah Forest Virus as Revealed by Cryo-Electron Microscopy at a 6-Angstrom Resolution Has Detailed Transmembrane Protein Architecture and Interactions. *J. Virol.* **2011**, *85*, 9327–9333.
22. Cheng, R. H.; Kuhn, R. J.; Olson, N. H.; Rossmann, M. G.; Choi, H. K.; Smith, T. J.; Baker, T. S. Nucleocapsid and Glycoprotein Organization in an Enveloped Virus. *Cell* **1995**, *80*, 621–630.
23. Sun, S.; Xiang, Y.; Akahata, W.; Holdaway, H.; Pal, P.; Zhang, X.; Diamond, M. S.; Nabel, G. J.; Rossmann, M. G. Structural Analyses at Pseudo Atomic Resolution of Chikungunya Virus and Antibodies Show Mechanisms of Neutralization. *eLife* **2013**, *2*, e00435.
24. Suomalainen, M.; Garoff, H. Alphavirus Spike-Nucleocapsid Interaction and Network Antibodies. *J. Virol.* **1992**, *66*, 5106–5109.
25. Tang, J.; Jose, J.; Chipman, P.; Zhang, W.; Kuhn, R. J.; Baker, T. S. Molecular Links between the E2 Envelope Glycoprotein and Nucleocapsid Core in Sindbis Virus. *J. Mol. Biol.* **2011**, *414*, 442–459.
26. Jose, J.; Przybyla, L.; Edwards, T. J.; Perera, R.; Burgner, J. W., 2nd; Kuhn, R. J. Interactions of the Cytoplasmic Domain of Sindbis Virus E2 with Nucleocapsid Cores Promote Alphavirus Budding. *J. Virol.* **2012**, *86*, 2585–2599.
27. Larkin, M. A.; Blackshields, G.; Brown, N. P.; Chenna, R.; McGettigan, P. A.; McWilliam, H.; Valentin, F.; Wallace, I. M.; Wilm, A.; Lopez, R.; *et al.* Clustal W and Clustal X Version 2.0. *Bioinformatics* **2007**, *23*, 2947–2948.
28. Garoff, H.; Frischauf, A. M.; Simons, K.; Lehrach, H.; Delius, H. The Capsid Protein of Semliki Forest Virus Has Clusters of Basic Amino Acids and Prolines in Its Amino-Terminal Region. *Proc. Natl. Acad. Sci. U. S. A.* **1980**, *77*, 6376–6380.
29. Bell, J. R.; Strauss, E. G.; Strauss, J. H. Purification and Amino Acid Compositions of the Structural Proteins of Sindbis Virus. *Virology* **1979**, *97*, 287–294.
30. Bell, J. R.; Bond, M. W.; Hunkapiller, M. W.; Strauss, E. G.; Strauss, J. H.; Yamamoto, K.; Simizu, B. Structural Proteins of Western Equine Encephalitis Virus: Amino Acid Compositions and N-Terminal Sequences. *J. Virol.* **1983**, *45*, 708–714.
31. Choi, H. K.; Tong, L.; Minor, W.; Dumas, P.; Boege, U.; Rossmann, M. G.; Wengler, G. Structure of Sindbis Virus Core Protein Reveals a Chymotrypsin-Like Serine Proteinase and the Organization of the Virion. *Nature* **1991**, *354*, 37–43.
32. Lee, S.; Owen, K. E.; Choi, H. K.; Lee, H.; Lu, G.; Wengler, G.; Brown, D. T.; Rossmann, M. G.; Kuhn, R. J. Identification of a Protein Binding Site on the Surface of the Alphavirus Nucleocapsid and Its Implication in Virus Assembly. *Structure* **1996**, *4*, 531–541.
33. Skoging, U.; Vihinen, M.; Nilsson, L.; Liljestrom, P. Aromatic Interactions Define the Binding of the Alphavirus Spike to Its Nucleocapsid. *Structure* **1996**, *4*, 519–529.
34. Mukhopadhyay, S.; Zhang, W.; Gabler, S.; Chipman, P. R.; Strauss, E. G.; Strauss, J. H.; Baker, T. S.; Kuhn, R. J.; Rossmann, M. G. Mapping the Structure and Function of the E1 and E2 Glycoproteins in Alphaviruses. *Structure* **2006**, *14*, 63–73.
35. Cheng, F.; Tsvetkova, I. B.; Khuong, Y. L.; Moore, A. W.; Arnold, R. J.; Goicochea, N. L.; Dragnea, B.; Mukhopadhyay, S. The Packaging of Different Cargo into Enveloped Viral Nanoparticles. *Mol. Pharmaceutics* **2013**, *10*, 51–58.
36. Goicochea, N. L.; De, M.; Rotello, V. M.; Mukhopadhyay, S.; Dragnea, B. Core-Like Particles of an Enveloped Animal Virus Can Self-Assemble Efficiently on Artificial Templates. *Nano Lett.* **2007**, *7*, 2281–2290.

37. Wengler, G.; Boege, U.; Wahn, K. Establishment and Analysis of a System Which Allows Assembly and Disassembly of Alphavirus Core-Like Particles under Physiological Conditions in Vitro. *Virology* **1984**, *132*, 401–412.
38. Wengler, G.; Wengler, G. In Vitro Analysis of Factors Involved in the Disassembly of Sindbis Virus Cores by 60s Ribosomal Subunits Identifies a Possible Role of Low Ph. *J. Gen. Virol.* **2002**, *83*, 2417–2426.
39. Wengler, G. The Regulation of Disassembly of Alphavirus Cores. *Arch. Virol.* **2009**, *154*, 381–390.
40. Wilkinson, T. A.; Tellinghuisen, T. L.; Kuhn, R. J.; Post, C. B. Association of Sindbis Virus Capsid Protein with Phospholipid Membranes and the E2 Glycoprotein: Implications for Alphavirus Assembly. *Biochemistry* **2005**, *44*, 2800–2810.
41. Snyder, J. E.; Azizgolshani, O.; Wu, B.; He, Y.; Lee, A. C.; Jose, J.; Suter, D. M.; Knobler, C. M.; Gelbart, W. M.; Kuhn, R. J. Rescue of Infectious Particles from Preassembled Alphavirus Nucleocapsid Cores. *J. Virol.* **2011**, *85*, 5773–5781.
42. Cheng, F.; Mukhopadhyay, S. Generating Enveloped Virus-Like Particles with in Vitro Assembled Cores. *Virology* **2011**, *413*, 153–160.
43. Katen, S. P.; Zlotnick, A. Thermodynamics of Virus Capsid Assembly. *Methods Enzymol.* **2009**, *455*, 395–417.
44. Paredes, A.; Alwell-Warda, K.; Weaver, S. C.; Chiu, W.; Watowich, S. J. Structure of Isolated Nucleocapsids from Venezuelan Equine Encephalitis Virus and Implications for Assembly and Disassembly of Enveloped Virus. *J. Virol.* **2003**, *77*, 659–664.
45. Singh, S.; Zlotnick, A. Observed Hysteresis of Virus Capsid Disassembly Is Implicit in Kinetic Models of Assembly. *J. Biol. Chem.* **2003**, *278*, 18249–18255.
46. Hagan, M. F.; Chandler, D. Dynamic Pathways for Viral Capsid Assembly. *Biophys. J.* **2006**, *91*, 42–54.
47. van der Schoot, P.; Zandi, R. Kinetic Theory of Virus Capsid Assembly. *Phys. Biol.* **2007**, *4*, 296–304.
48. Uetrecht, C.; Watts, N. R.; Stahl, S. J.; Wingfield, P. T.; Steven, A. C.; Heck, A. J. Subunit Exchange Rates in Hepatitis B Virus Capsids Are Geometry- and Temperature-Dependent. *Phys. Chem. Chem. Phys.* **2010**, *12*, 13368–13371.
49. Zhang, W.; Mukhopadhyay, S.; Pletnev, S. V.; Baker, T. S.; Kuhn, R. J.; Rossmann, M. G. Placement of the Structural Proteins in Sindbis Virus. *J. Virol.* **2002**, *76*, 11645–11658.
50. Coombs, K.; Brown, B.; Brown, D. T. Evidence for a Change in Capsid Morphology During Sindbis Virus Envelopment. *Virus Res.* **1984**, *1*, 297–302.
51. Sokoloski, K. J.; Snyder, A. J.; Liu, N. H.; Hayes, C. A.; Mukhopadhyay, S.; Hardy, R. W. Encapsidation of Host-Derived Factors Correlates with Enhanced Infectivity of Sindbis Virus. *J. Virol.* **2013**, *87*, 12216–12226.
52. Geigenmuller-Gnirke, U.; Nitschko, H.; Schlesinger, S. Deletion Analysis of the Capsid Protein of Sindbis Virus: Identification of the Rna Binding Region. *J. Virol.* **1993**, *67*, 1620–1626.
53. Owen, K. E.; Kuhn, R. J. Identification of a Region in the Sindbis Virus Nucleocapsid Protein That Is Involved in Specificity of Rna Encapsidation. *J. Virol.* **1996**, *70*, 2757–2763.
54. Warrier, R.; Linger, B. R.; Golden, B. L.; Kuhn, R. J. Role of Sindbis Virus Capsid Protein Region Ii in Nucleocapsid Core Assembly and Encapsidation of Genomic Rna. *J. Virol.* **2008**, *82*, 4461–4470.
55. Zandi, R.; Reguera, D. Mechanical Properties of Viral Capsids. *Phys. Rev. E: Stat., Nonlinear, Soft Matter Phys.* **2005**, *72*, 021917.
56. Forsell, K.; Xing, L.; Kozlovska, T.; Cheng, R. H.; Garoff, H. Membrane Proteins Organize a Symmetrical Virus. *EMBO J.* **2000**, *19*, 5081–5091.
57. Mukhopadhyay, S.; Kim, B. S.; Chipman, P. R.; Rossmann, M. G.; Kuhn, R. J. Structure of West Nile Virus. *Science* **2003**, *302*, 248.
58. Pokidysheva, E.; Zhang, Y.; Battisti, A. J.; Bator-Kelly, C. M.; Chipman, P. R.; Xiao, C.; Gregorio, G. G.; Hendrickson, W. A.; Kuhn, R. J.; Rossmann, M. G. Cryo-Em Reconstruction of Dengue Virus in Complex with the Carbohydrate Recognition Domain of Dc-Sign. *Cell* **2006**, *124*, 485–493.
59. Glotzer, S. C.; Solomon, M. J. Anisotropy of Building Blocks and Their Assembly into Complex Structures. *Nat. Mater.* **2007**, *6*, 557–562.
60. Luque, A.; Reguera, D.; Morozov, A.; Rudnick, J.; Bruinsma, R. Physics of Shell Assembly: Line Tension, Hole Implosion, and Closure Catastrophe. *J. Chem. Phys.* **2012**, *136*, 184507.
61. Snyder, A. J.; Mukhopadhyay, S. The Alphavirus E3 Glycoprotein Functions in a Clade-Specific Manner. *J. Virol.* **2012**, *86*, 13609–13620.
62. Wang, J. C.; Dhason, M. S.; Zlotnick, A. Structural Organization of Pregenomic Rna and the Carboxy-Terminal Domain of the Capsid Protein of Hepatitis B Virus. *PLoS Pathog.* **2012**, *8*, e1002919.
63. Yan, X.; Sinkovits, R. S.; Baker, T. S. Auto3dem - an Automated and High Throughput Program for Image Reconstruction of Icosahedral Particles. *J. Struct. Biol.* **2007**, *157*, 73–82.
64. Tang, G.; Peng, L.; Baldwin, P. R.; Mann, D. S.; Jiang, W.; Rees, I.; Ludtke, S. J. Eman2: An Extensible Image Processing Suite for Electron Microscopy. *J. Struct. Biol.* **2007**, *157*, 38–46.
65. Yan, X.; Sinkovits, R. S.; Baker, T. S. Auto3dem--an Automated and High Throughput Program for Image Reconstruction of Icosahedral Particles. *J. Struct. Biol.* **2007**, *157*, 73–82.
66. Pettersen, E. F.; Goddard, T. D.; Huang, C. C.; Couch, G. S.; Greenblatt, D. M.; Meng, E. C.; Ferrin, T. E. Ucsf Chimera--a Visualization System for Exploratory Research and Analysis. *J. Comput. Chem.* **2004**, *25*, 1605–1612.
67. Sorzano, C. O.; Marabini, R.; Velazquez-Muriel, J.; Bilbao-Castro, J. R.; Scheres, S. H.; Carazo, J. M.; Pascual-Montano, A. Xmipp: A New Generation of an Open-Source Image Processing Package for Electron Microscopy. *J. Struct. Biol.* **2004**, *148*, 194–204.
68. Ludtke, S. J.; Baldwin, P. R.; Chiu, W. Eman: Semiautomated Software for High-Resolution Single-Particle Reconstructions. *J. Struct. Biol.* **1999**, *128*, 82–97.